

BAYESIAN AGES FOR EARLY-TYPE STARS FROM ISOCHRONES INCLUDING ROTATION, AND A POSSIBLE OLD AGE FOR THE HYADES

TIMOTHY D. BRANDT^{1, 3} & CHELSEA X. HUANG²*Draft version April 2, 2022*

ABSTRACT

We combine recently computed models of stellar evolution using a new treatment of rotation with a Bayesian statistical framework to constrain the ages and other properties of early-type stars. We find good agreement for early-type stars and clusters with known young ages, including β Pictoris and the Pleiades. However, we derive a slightly older age for the Ursa Majoris moving group (600 ± 100 Myr compared to 500 ± 100 Myr), and a much older age for the Hyades open cluster (950 ± 100 Myr compared to 625 ± 50 Myr). These older ages result from both the increase in main-sequence lifetime with stellar rotation and from the fact that rotating models near the main-sequence turnoff are more luminous, overlapping with slightly more massive (and shorter-lived) nonrotating ones. The dramatically older age inferred for the Hyades requires a major reevaluation either of the cluster age or of the rotating stellar models. Our method uses a large grid of nonrotating models to interpolate between a much sparser rotating grid, and also includes a detailed calculation of synthetic magnitudes as a function of orientation. We provide a web interface at www.bayesianstellarparameters.info, where the results of our analysis may be downloaded for individual early-type ($B-V \lesssim 0.25$) *Hipparcos* stars. The web interface accepts user-supplied parameters for a Gaussian metallicity prior and returns posterior probability distributions on mass, age, and orientation.

Subject headings:

1. INTRODUCTION

Stellar ages are important in many areas of astrophysics, from understanding the evolution of galaxies, to chemical enrichment, to the properties of planetary systems. They are also usually inaccessible by direct measurement and must be obtained by fitting to models (Soderblom 2010). The one exception is the Sun, radiometrically dated from inclusions in meteorites (Connelly et al. 2012). Stars older than ~ 100 Myr may be dated by fitting models of stellar evolution (Perryman et al. 1998; Takeda et al. 2007) or by using calibrated empirical methods like lithium depletion (Sestito & Randich 2005) or the decline of activity and rotation (Noyes et al. 1984; Barnes 2007; Mamajek & Hillenbrand 2008). These empirical methods are calibrated at ages of several hundred Myr using clusters dated by fitting model isochrones.

Low-mass field stars may be reliably dated by the decline of their rotation and activity. FGK stars develop an outer convective zone, generating a magnetic field and driving a wind that carries away angular momentum (Parker 1955; Glatzmaier 1985). They spin down and become less chromospherically and coronally active with age (Wilson 1963; Hempelmann et al. 1995), providing a clock that can give ages to $\sim 20\%$ (Mamajek & Hillenbrand 2008). Isochrone fits to coeval clusters are used to calibrate the empirical rotation and activity relations at ages of several hundred Myr. The accuracy and precision of gyrochronology ages thus rely on the those of isochrone fits.

Stars more massive than $\sim 1.3 M_{\odot}$ have radiative en-

velopes and convective cores, and retain their angular momentum throughout the main sequence (Barnes 2003). Even individual early-type stars are typically dated by fitting model isochrones (e.g. Zorec & Royer 2012; Nielsen et al. 2013). Given an initial mass and metallicity, stellar evolution models predict the stellar radius and luminosity as a function of time. Together with a model atmosphere, theoretical isochrones can be used to generate a grid of luminosities in each band as a function of initial mass, metallicity, and age. A star's distance and fluxes can then be inverted to give a mass, metallicity, and age. Unfortunately, the inversion is often not unique, with multiple paths in the color-magnitude diagram crossing one another (Soderblom 2010).

Models of stellar evolution are subject to a very wide range of uncertainties, from the treatment of convection and overshooting, to the composition and opacities, to the treatment of rotation. Rotation, in particular, can introduce moderate changes in luminosity, color and brightness variations with viewing angle, and large, $\sim 25\%$ increases in the main-sequence lifetime as rotationally-induced mixing supplies the core with fresh hydrogen (Ekström et al. 2012). The dependence of main-sequence lifetime on rotation can broaden the main-sequence and especially the main-sequence turnoff (Georgy et al. 2014; Li et al. 2014), mimicking the effect of a spread of ages. The effects of rotation are most important for stars that do not brake magnetically, i.e., stars $\gtrsim 1.3 M_{\odot}$. These are precisely the stars for which isochrone dating is the most important, and often the only, way of estimating their age.

In this paper, we perform isochrone dating of early-type stars using a recent set of stellar models with a shellular treatment of rotation (Georgy et al. 2013b). These models cover a range of metallicities from $Z_{\odot} = 0.002$

¹ School of Natural Sciences, Institute for Advanced Study, Princeton, NJ, USA.

² Department of Astrophysical Sciences, Princeton University, Princeton, NJ, USA.

³ NASA Sagan Fellow

to $Z = 0.014$, initial rotation rates from 0 to 95% of breakup, and masses from $1.7 M_{\odot}$ to $15 M_{\odot}$. We use a much finer grid of nonrotating stellar models (Girardi et al. 2002) to interpolate between the rotating models, and to extrapolate to $1.45 M_{\odot}$ and to $Z = 0.04$. The extrapolations rely on the fact that the additional effects of rotation in these models depend only weakly on mass and metallicity. We use a Roche model of the star (Espinosa Lara & Rieutord 2011) together with the ATLAS9 model atmospheres (Castelli & Kurucz 2004) to compute synthetic photometry for each stellar model as a function of orientation. We then adopt a Bayesian framework to constrain stellar parameters.

We organize our paper as follows. In Section 2 we describe our Bayesian statistical formalism, while in Section 3 we describe the stellar models that we use and the effects of adding rotation. In Section 4 we describe our use of the Roche model of a star together with model atmospheres to compute synthetic photometry. In Section 5 we apply our method to four nearby early-type stars and to two coeval associations, UMa and the Hyades. We conclude with Section 6.

2. STATISTICAL FRAMEWORK

The likelihood of a stellar evolution model is the probability of measuring the observed fluxes and distance given the predicted luminosities in each band:

$$\mathcal{L}(M, Z, \tau, \varpi) = p(\{m_j, \varpi_{\text{obs}}\} | \{M_j(M, Z, \tau), \varpi\}) , \quad (1)$$

where M is the model's mass, Z its metallicity and τ its age, ϖ is the parallax, m_j are the apparent magnitudes in bands j , and M_j are the (absolute) model magnitudes. The addition of rotation in stellar models enables us to include the measured projected rotational velocity, $v \sin i$, in the likelihood function. Stellar rotation also modifies the main sequence lifetime, apparent luminosity, and colors, which all become functions of the angular velocity Ω and inclination i ($i = 0$ denoting pole-on). These become additional parameters in Equation (1) upon which the M_j depend.

For convenience, and for lack of an obvious alternative, we assume that the errors in observed magnitudes are Gaussian. We neglect errors in the synthetic photometry apart from a possible systematic error that we add in quadrature to the photometric errors. Such a systematic error is best interpreted as a color uncertainty. The error in the *Hipparcos* parallax (which we also assume to be Gaussian) is typically a few percent for nearby stars (van Leeuwen 2007), which is equivalent to much more than a 1% uncertainty in flux. With these assumptions and simplifications, the likelihood function becomes

$$\begin{aligned} -2 \ln \mathcal{L} = & \sum_{\text{bands } j} \frac{(M_{\text{mod},j}(\mu, \Omega) + 5 \log_{10} 100/\varpi - m_{\text{obs},j})^2}{\sigma_i^2} \\ & + \frac{(\varpi - \varpi_{\text{obs}})^2}{\sigma_{\varpi}^2} + \frac{(R_{\text{eq}} \Omega \sin i - v_{\text{obs}})^2}{\sigma_v^2} , \quad (2) \end{aligned}$$

where $M_{\text{mod},j}$ is the model absolute magnitude in band j , ϖ is the parallax in milliarcseconds, $R_{\text{eq}} \Omega$ is the model equatorial velocity, and v_{obs} is the observed projected rotational velocity.

In a Bayesian framework, the posterior probability of the model is the product of the likelihood and the prior

probability of the model parameters: Z, M_0, τ, ϖ, i and Ω :

$$p(M, Z, \tau, \Omega, i) \propto p(M)p(Z)p(\tau)p(i)p(\Omega)\mathcal{L}(M, Z, \tau, \Omega, i) . \quad (3)$$

The appropriate priors on M_0, τ, ϖ , and i are all well-established: uniform in volume and time, and proportional to the initial mass function (IMF). The prior on parallax is thus $dp/d\varpi \propto \varpi^{-4}$, while $dp/di = \sin i$, where $i = 0$ denotes a polar viewing angle. We adopt a Salpeter IMF, $dp/dM \propto M^{-2.35}$, appropriate for stars $\gtrsim 1 M_{\odot}$ (Salpeter 1955; Kroupa 2001; Chabrier 2003).

An appropriate prior on Z in the absence of other information about the star may be taken from the metallicities of nearby young stars. There is some disagreement on the chemical composition of the young Solar neighborhood. The large spectroscopic sample of Casagrande et al. (2011) implies a slightly sub-Solar mean metallicity for young stars, and a dispersion ~ 0.1 dex. This may disagree with Przybilla et al. (2008) and Nieva & Przybilla (2012), who compared high resolution, high signal-to-noise ratio spectra of twenty nearby early B stars to detailed atmospheric models. Nieva & Przybilla (2012) found abundances almost identical to those of the Solar photosphere (Asplund et al. 2009), with a scatter of just $\sim 10\%$, or 0.03 dex, even when including measurement uncertainties. These results are in much better agreement with models of Galactic chemical enrichment and mixing in the interstellar medium (Roy & Kunth 1995; Chiappini et al. 2003). The data in Casagrande et al. (2011) also show some trends that are unlikely to be real, including a correlation of metallicity with stellar mass at fixed age (their Figure 16). We suggest a Gaussian prior centered on $[\text{Fe}/\text{H}] = 0$ with a dispersion of 0.1 dex as a very conservative (perhaps overly conservative) choice.

Our suggested metallicity prior is problematic for chemically peculiar early-type stars. These stars are expected to have unremarkable bulk compositions, but atmospheres heavily influenced by diffusion and/or magnetic fields (Preston 1974; Smith 1996). Individual elements and groups of elements can be over- or under-abundant by factors of tens or hundreds. Chemically peculiar stars are relatively common on the upper main sequence, and our results for them must be interpreted with caution. Such stars should be perhaps be fitted by a stellar model with different bulk and atmospheric compositions.

The prior on stellar rotation is more difficult to determine. Stellar evolution codes calculate a star's structure throughout its main-sequence life, which can entail a significant redistribution of its angular momentum. The only free parameter in this case is a star's *initial* supply of angular momentum, which need not be represented by its observed equatorial velocity (and which is shed in a magnetized wind by stars $\lesssim 1.3 M_{\odot}$). An appropriate prior probability on rotation would be the distribution of angular momentum (or equatorial velocity, often the only observable) for young early-type stars, which do not shed angular momentum.

Zorec & Royer (2012) have estimated the evolution of equatorial velocity for stars in various mass bins at different stages of evolution. For ~ 1.5 – $3 M_{\odot}$ stars early in their main-sequence lifetimes, Zorec & Royer find peaks in the rotational velocities consistent with a bimodal dis-

tribution. The first peak is at low velocities while the second, which accounts for most of the stars, may be approximated by a lagged Maxwellian with a mode of $\Omega/\Omega_{\text{crit}} \sim 0.4$. Their analysis also hints that $\Omega/\Omega_{\text{crit}}$ may increase somewhat with initial stellar mass.

We use the models of Georgy et al. (2013b) in our analysis, which have equatorial $\Omega/\Omega_{\text{crit}}$ somewhat lower than the initial values at which the models are tabulated. We therefore use distributions in $\Omega/\Omega_{\text{crit}}$ peaking at somewhat larger values than those derived by Zorec & Royer (2012). For simplicity, we use a simple Maxwellian distribution with a mode of 0.5 truncated at 0.95. This captures the essential elements of the data Zorec & Royer analyze, apart from a few (~ 0 –20%, depending on mass) of stars that appear to rotate slowly, and reproduces the approximate upper limits to observed values of $v \sin i$.

3. STELLAR EVOLUTION MODELS WITH ROTATION

A wide range of stellar evolution models is now available, covering fine grids of mass, metallicity, and time (Yi et al. 2001; Girardi et al. 2002; Pietrinferni et al. 2004; Dotter et al. 2008). Some models, going back more than a decade, have included rotation (Meynet & Maeder 2000). The addition of rotation turns a 1D stellar structure into at least a 2D structure. This is simplified in practice with assumptions like that of “shellular” rotation (Zahn 1992), in which the angular velocity is constant along isobars. Rotation is relatively unimportant for stars below $\sim 1.3 M_{\odot}$, which spin down rapidly. However, it can introduce large effects for stars with radiative envelopes (Meynet & Maeder 2000), perhaps most notably an increase in time spent on the main sequence.

Stellar modeling includes a very wide range of tunable physical parameters governing everything from the chemical abundances and their opacities, to the treatment of convection, to the treatment (or lack) of rotation, to the model atmospheres. These parameters and treatments vary from one set of stellar models to another and can lead to significant variations in colors, luminosities, and lifetimes (Lebreton et al. 2014). For the rest of this analysis, we adopt the models of Georgy et al. (2013a) as our primary source, compute synthetic photometry ourselves, and neglect uncertainties in parameters like the helium fraction or convective overshooting.

The recent stellar evolution models of Ekström et al. (2012) and Georgy et al. (2013a) include both rotating and non-rotating stars, in the former case covering a range of initial rotation rates and metallicities. These grids are, however, very coarse, and only extend to $Z = Z_{\odot}$. We therefore use much finer grids of nonrotating models to interpolate between the rotating models, and to extrapolate them to higher metallicities. We adopt the PARSEC isochrones (Girardi et al. 2002) for this interpolation. Because we anchor them to the Georgy et al. (2013a) models, the details of the PARSEC calculations are unimportant here. Any effects that are linearly dependent on mass and metallicity will disappear entirely.

The validity of our interpolation and extrapolation relies on the fact that the modifications to stellar evolution provided by rotation depend only weakly on other stellar parameters. In this analysis, we restrict the models to $M > 1.5 M_{\odot}$, for which magnetic braking is inefficient

and rotation is important throughout the main sequence. We apply our upper mass cutoff at $11 M_{\odot}$, which has a main sequence lifetime of just a few tens of Myr.

The rapidly rotating stellar models have main-sequence lifetimes that depend strongly on Ω , the initial angular momentum. Interpolating with nonrotating models requires us to introduce a dimensionless time, t/t_{MS} , the ratio of the stellar age to its main sequence lifetime. The parameter t_{MS} is a function of stellar rotation:

$$t_{\text{MS}} = t_{\text{MS, nr}} \beta(M_0, \Omega) . \quad (4)$$

We use the PARSEC models to interpolate $t_{\text{MS, nr}}$ between masses in the Geneva models, and separately interpolate β , which depends very weakly on mass and metallicity. We note that the nonrotating PARSEC isochrones do differ significantly from the nonrotating Geneva models. For example, 1.5–5 M_{\odot} PARSEC models spend $\sim 10\%$ longer on the main sequence than the corresponding Geneva models we use here.

The other effects of rotation include an increase in luminosity and a flattening of the stellar surface, which make the apparent luminosity of the star a function of viewing angle. We describe the computation of synthetic photometry in the following section. To interpolate between models, we separate the photometry into nonrotating magnitudes and a rotating correction as a function of Ω , photometric band, and inclination. These two components are additive in units of magnitude (multiplicative in units of flux). We then use the PARSEC models to interpolate the nonrotating synthetic photometry between Geneva models. We separately interpolate or extrapolate the rotation correction term, which, like β from Equation (4), depends only weakly on stellar mass and metallicity. This interpolation in linear in units of magnitude.

4. COMPUTING THE EFFECT OF ORIENTATION

Stellar oblateness introduces two effects: a viewer along the pole sees a star both larger in area and hotter. In all bands, the star will therefore appear more luminous with decreasing inclination i ($i = 0$ denoting a line-of-sight parallel to the polar axis), except when i approaches 0° and the gravity darkening effect is severe. The variation of stellar surface brightness with latitude is a consequence of the von Zeipel theorem (von Zeipel 1924), which states that the local effective temperature depends on the local effective gravity as a power-law $T_{\text{eff}} \propto g_{\text{eff}}^{\beta}$, with β known as the gravity darkening coefficient. The original von Zeipel law states $\beta = 1/4$ for stars with fully radiative envelopes. Generally, β is smaller than $1/4$, as discovered by recent interferometric observations of rapidly rotating nearby stars (Aufdenberg et al. 2006; van Belle et al. 2006).

Although comprehensive calculations of β were carried out by Claret (1998) for stars at different evolutionary stages, we choose to adopt a two-dimensional model developed by Espinosa Lara & Rieutord (2011) (hereafter LR11), in which the effective temperature profile only depends on the ratio of the equatorial velocity and the Keplerian velocity $w = \Omega/\Omega_{\text{crit}}$. This parameter is supplied by the stellar evolution models (Ekström et al. 2012). With the total luminosity, oblateness, and radius from the stellar models, we can compute T_{eff} and g_{eff} over the entire stellar surface. Finally, we use the specific intensi-

ties from the ATLAS9 models (Castelli & Kurucz 2004) to integrate the apparent flux through a series of filters as a function of viewing angle.

4.1. Computing Fluxes

We follow Section 2 of LR11 to compute the effective temperature map over the stellar surface. The assumption of the model can be simply stated as the following: the mass distribution of the star may be described as a Roche model, and the energy flux is a divergence-free vector that is almost anti-parallel to the effective gravity. The effective temperature profile at a particular polar angle θ can then be expressed as

$$T_{\text{eff}} = \left(\frac{1}{r^4} + w^4 r^2 \sin^2 \theta - \frac{2w^2 \sin^2 \theta}{r} \right)^{1/8} \times \left(\frac{L}{4\pi\sigma R_{\text{eq}}^2} \right)^{1/4} F_w^{1/4}, \quad (5)$$

in which r is the radius at the stellar surface in units of the equatorial radius R_{eq} , w is the ratio between the equatorial velocity and the Keplerian velocity $\Omega/\Omega_{\text{crit}}$, and F_w is a correction factor that takes into account the difference between the vector angle of energy flux and the effective gravity. When the rotation is slow ($R_{\text{pole}}/R_{\text{eq}} > 0.95$), $F_w = 1$, and this model reduces to the von Zeipel case.

We solve for F_w numerically using a combined Newton-Raphson and bisection method following Equations (24)–(28) of LR11. The stellar surface is assumed to be an oblate ellipsoid with $a = R_{\text{eq}}$ and $c = R_{\text{pol}}$. The projection of the stellar surface onto the plane of the sky with an inclination i is an ellipse with $a = R_{\text{eq}}$ and $b = (R_{\text{eq}}^2 R_{\text{pol}}^2) / (R_{\text{eq}}^2 \cos^2 i + R_{\text{pol}}^2 \sin^2 i)$.

We use the ATLAS9 stellar atmosphere models (Castelli & Kurucz 2004) to compute the specific intensities, and the Tycho, 2MASS (Cutri et al. 2003), and Johnson-Cousins filter response curves to compute photon fluxes at a distance of 10 pc. We adopt the recently revised *Tycho* responses (Bessell & Murphy 2012), which differ slightly (by $\lesssim 5$ mmag in $B_T - V_T$) from those originally published (ESA 1997). The abundances in the ATLAS9 models are relative to Anders & Grevesse (1989), which gives a Solar metallicity $Z = 0.019$. This is higher by 0.10–0.13 dex than the Z_{\odot} values adopted by Girardi et al. (2002) and Ekström et al. (2012) based on the abundances measured by Asplund et al. (2009). We therefore use the ATLAS9 models with $[\text{Fe}/\text{H}] = -0.1$ for the isochrone models at solar metallicity.

Our adoption of $Z_{\odot} \approx 0.014$ could introduce systematic effects when using spectroscopic metallicities that assume a different Z_{\odot} . As a result, $[\text{Fe}/\text{H}] = 0.1$ in this work could correspond in some ways to a spectroscopic $[\text{Fe}/\text{H}] = 0.0$. Our scaling of the Anders & Grevesse (1989) photospheric composition does, however, mean that the composition of the stellar atmosphere roughly matches the bulk composition of the star.

4.2. A Parametrized Fit

Our method allows us to compute the magnitudes in all bands as a function of orientation. We wish to use the fine grid of nonrotating PARSEC isochrones (Girardi

et al. 2002) to interpolate within the coarse grid of rotating Geneva models. We therefore compute the difference in magnitude between the rapidly rotating models of Georgy et al. (2013b) and PARSEC models at the same mass, metallicity, and fraction of main sequence lifetime. Some of the Georgy et al. (2013b) models are computed with zero initial angular momentum. These models are not identical to the corresponding PARSEC models; for example, nonrotating PARSEC $\sim 2 M_{\odot}$ stars typically spend $\sim 10\%$ longer on the main sequence than the corresponding nonrotating Geneva models. Even at zero rotation, the difference between Geneva and PARSEC model magnitudes can be significant.

We compute the magnitude corrections as a function of viewing angle $\mu \equiv \cos i$ ($\mu = 1$ corresponding to pole-on). We then fit a polynomial in μ for each band and rotating model,

$$M(\mu \equiv \cos i) = M_{\text{PARSEC}} + \sum_{i=0}^n a_i \mu^i. \quad (6)$$

Figure 1 shows the residuals from this fitting function for the Johnson-Cousins U passband as a function of T_{eff} and obliquity at an equatorial $\log g = 4$. We obtain excellent agreement with $n = 5$, with residuals $\lesssim 1$ mmag for all but the coolest models at the fastest rotations. These residuals decrease towards longer-wavelength passbands. With $n = 5$, they are typically at least an order of magnitude smaller than the photometric measurement errors, and likely smaller than errors resulting from interpolation between isochrones.

The a_i in Equation (6) are functions of the band, stellar mass, rotation rate, metallicity, and age, and are logarithmic in the stellar flux. We linearly interpolate (and even extrapolate, in metallicity), these parameters onto the fine nonrotating PARSEC grids. In doing so, we take advantage of the fact that while the stellar models themselves may depend strongly on physical parameters like mass and metallicity, the a_i correction coefficients have a much weaker dependence.

With the effect of rotation reduced to the parameters of Equation (6), we can compute the effects of both rotation and orientation on observed colors and magnitudes. Figure 2 shows both nonrotating and rotating isochrones (with $\Omega/\Omega_{\text{crit}} = 0.5$) at a series of representative ages. A rotating model at fixed age actually covers a line in the color-magnitude diagram, as much as ~ 0.1 – 0.2 magnitudes in V and 0.05 magnitudes in $B - V$ (the navy blue lines in the figure). At very young ages, the effect of rotation is modest. At older ages, however, a rotating stellar model will overlap a significantly younger and slightly more massive model in color-magnitude space. The combination of an increased luminosity at a similar $B - V$ color with a longer time spent on the main sequence can have a very large effect on isochrone ages using main-sequence turnoff stars. This is especially apparent for the Hyades open cluster, which we discuss at the end of the next section.

5. RESULTS

In the following subsections we present the results of our isochrone analysis for a selection of A and B stars. We apply it first to a series of three individual stars of

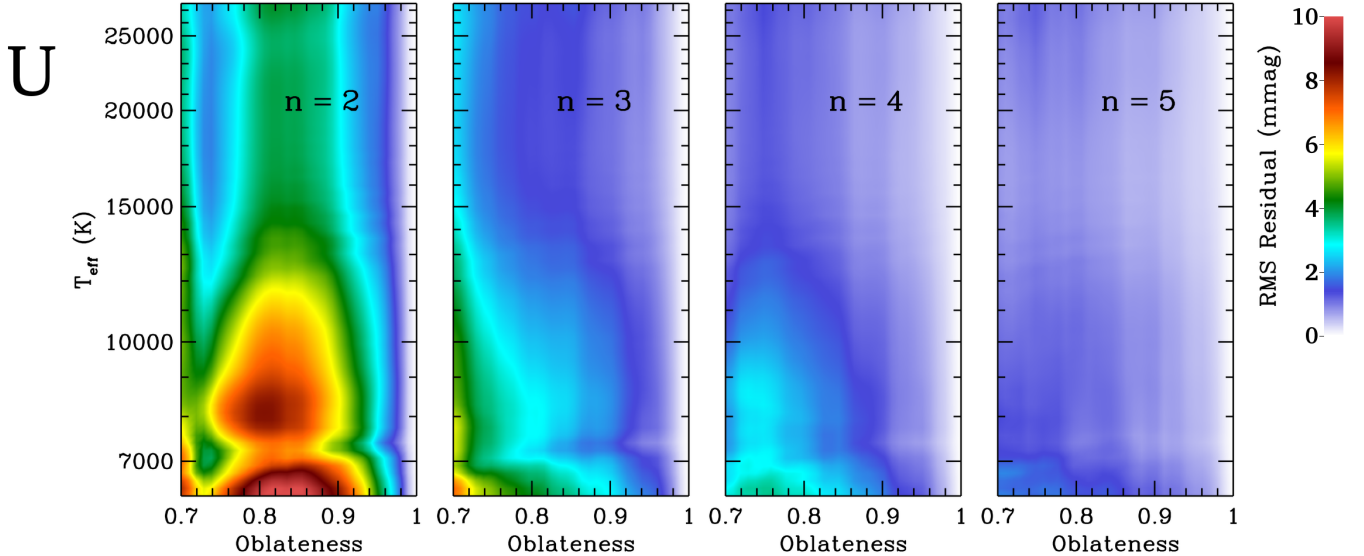


FIG. 1.— Distribution of the residuals from Equation (6) for the Johnson-Cousins U -band. With a fitting polynomial of order $n = 5$, the root-mean-square residuals are $\lesssim 1$ mmag for all but the lowest temperature, most rapidly rotating stars. This is much less than pole-equator differences reaching 0.1 mag or more, and less than errors due to interpolation and measurement errors. The residuals are smaller still (i.e. the fit is better) at the longer-wavelength passbands that we use.

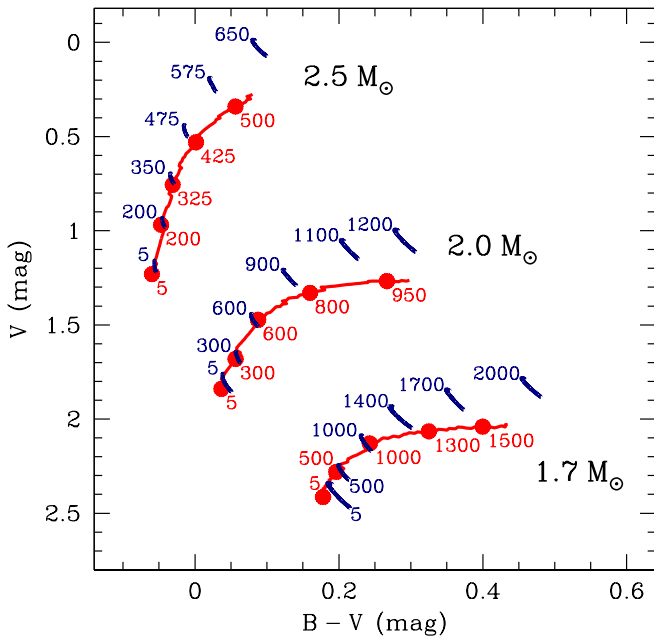


FIG. 2.— Isochrones for three stellar masses, with (blue) and without (red) rotation at fixed $\Omega/\Omega_{\text{crit}} = 0.5$; several ages are noted in Myr. The rotating models have been plotted only at representative ages to show the effects of orientation. The lines show the positions in color-magnitude space as a function of orientation. At older ages, a rotating model will overlap a significantly younger, slightly more massive nonrotating star in color-magnitude space.

known age and to one star, κ And, with an imaged sub-stellar companion and a controversial age. We have generally excluded close visual and spectroscopic binaries but have not excluded any stars based on the performance of our fitting. We then apply our isochrone-based analysis to two stellar clusters with previously inferred

isochrone ages, the Ursa Majoris moving group and the Hyades open cluster.

We restrict our analyses to the *Tycho-2* B_T and V_T photometry (Høg et al. 2000). These data have been well-calibrated and offer precisions of ~ 0.01 mag down to $V_T \sim 8$ over the entire sky. 2MASS JHK_s photometry could also be used, but would require a careful analysis demonstrating its calibration relative to *Tycho* at levels of $\lesssim 0.01$ mag, and a demonstration that the model atmospheres are adequate over such a wide range of wavelengths. We defer such an investigation to a future paper. We use *Hipparcos* parallaxes throughout (van Leeuwen 2007), and use $v \sin i$ measurements collected and calibrated by Zorec & Royer (2012).

In all of our fitting, we apply floors on the measurement errors of all parameters, which we add in quadrature with the actual reported uncertainties. These error floors are 0.005 magnitudes in all bands ($\sim 0.5\%$ in flux), which are best thought of as color errors, and 30 km s^{-1} in $v \sin i$. They are designed to minimize the impact of the coarseness of our model grid and to account for some uncertainties in the synthetic photometry. The Geneva models are only computed at nine initial angular momenta; the spacing between them corresponds to ~ 20 – 50 km s^{-1} in equatorial velocity. The spacing between neighboring models in luminosity is typically $\sim 2\%$ (and typically much less in color). The difference in synthetic colors between the original and recalibrated *Tycho* photometric system produces a systematic shift in $B_T - V_T$ of ~ 0.004 mag, while errors in parallax are $\gtrsim 2\%$.

When fitting an ensemble of stars that share an age and chemical composition, we multiply the two-dimensional posterior probability distributions for each individual star. This relies on the stellar models providing adequate fits to all stars, and on these fits being consistent. A rigorous statistical statement of consistency depends on the actual distributions. Roughly speaking, however,

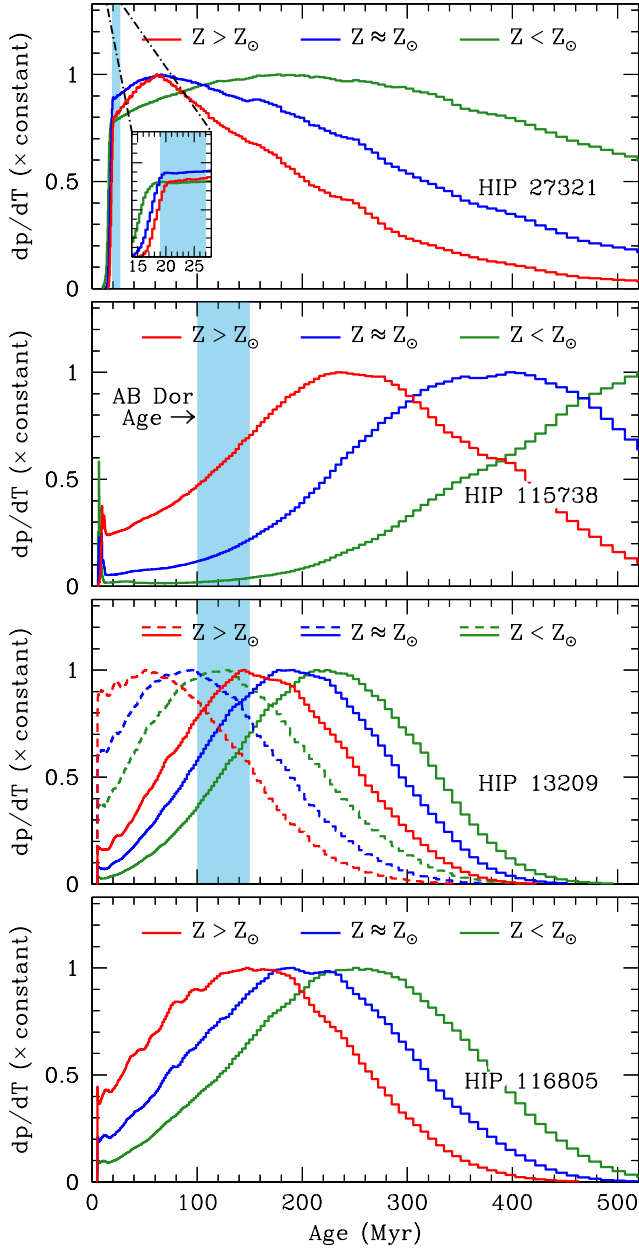


FIG. 3.— Posterior age probability distributions for four Hipparcos stars, each with three metallicity priors: $[\text{Fe}/\text{H}] = 0.1 \pm 0.05$ (red histograms), $[\text{Fe}/\text{H}] = 0 \pm 0.05$ (blue histograms), and $[\text{Fe}/\text{H}] = -0.1 \pm 0.05$ (green histograms). HIP 13209 (third panel) has a binary companion of unknown spectral type. The solid curves show the age distributions assuming no companion, while the dashed lines assume an F6V companion (with the luminosity of π^3 Ori). The shaded light blue regions show the moving group ages of the top three stars. Slightly super-Solar metallicities allow an excellent match in these cases. HIP 116805’s age is controversial; our analysis suggests that youth cannot be ruled out.

consistency requires that the 1σ contour of the multiplied posterior distribution be at a level comparable to the product of the 1σ contours in each individual distribution. All of our cluster probability distributions presented below easily pass this test.

5.1. Single Stars

We first apply our isochrone-based analysis to four individual stars: HIP 27321 (β Pictoris), 13209, 115738,

and 116805 (κ And). The first three of these stars are consensus members of the coeval moving groups β Pictoris (HIP 27321) and AB Doradus (HIP 13209 and 115738). HIP 116805 is a proposed member of the Columba moving group, but this identification, and the star’s age, are controversial. Figure 3 shows the age posterior probability distributions for each of these stars for three Gaussian metallicity distributions: $[\text{Fe}/\text{H}] = 0.1 \pm 0.05$ (red histograms), $[\text{Fe}/\text{H}] = 0 \pm 0.05$ (blue histograms), and $[\text{Fe}/\text{H}] = -0.1 \pm 0.05$ (green histograms). The shaded blue regions show the moving group ages. We discuss each star in turn below.

HIP 27321: The nearby A star β Pictoris hosts a debris disk and a low-mass substellar companion (Lagrange et al. 2009). It is also the founding member of the β Pictoris moving group (Barrado y Navascués et al. 1999; Zuckerman et al. 2001), whose age has recently been determined to be ~ 20 – 25 Myr using the lithium depletion boundary, isochrones with magnetic fields, and kinematics (Binks & Jeffries 2014; Malo et al. 2014; Mamajek & Bell 2014).

HIP 27321 has a measured rotational velocity of ~ 120 – 130 km s^{-1} (Royer et al. 2007; Schröder et al. 2009) and, while measurements of its metallicity are unreliable, we can adopt the chemical composition of lower-temperature members of the same moving group. HIP 10679 has a spectroscopic $[\text{Fe}/\text{H}] = 0.07 \pm 0.03$, HIP 10680 has $[\text{Fe}/\text{H}] = 0.09 \pm 0.03$, and HIP 25486 has $[\text{Fe}/\text{H}] = 0.29 \pm 0.03$ (Valenti & Fischer 2005). As members of the same moving group, these stars should have nearly identical compositions. The inconsistency between their spectroscopic metallicities in the same survey could indicate large systematic errors. The measurements do, however, hint at a slightly super-solar $[\text{Fe}/\text{H}]$ for β Pic itself.

The top panel of Figure 3 shows the age posterior probability distribution for HIP 27321 under three metallicity priors. The red histogram, $[\text{Fe}/\text{H}] = 0.1 \pm 0.05$, comes closest to the metallicities determined for later-type β Pic members, and correctly indicates a young age for HIP 27321 itself. The lower limit on the star’s age (shown in detail in the inset) reflects the pre-main sequence contraction time in the PARSEC isochrones (Girardi et al. 2002).

HIP 115738: HIP 115738 is an α^2 CVn variable star, and a high-probability member of the AB Doradus moving group (Zuckerman et al. 2011; Malo et al. 2013; Gagné et al. 2014), with an age of ~ 100 – 150 Myr (Luhman et al. 2005; Ortega et al. 2007; Barenfeld et al. 2013). The metallicity of AB Dor is somewhat uncertain, with measurements of $[\text{Fe}/\text{H}] = 0.02 \pm 0.02$ (Barenfeld et al. 2013) and $[\text{Fe}/\text{H}] = 0.10 \pm 0.03$ (Biazzo et al. 2012), from spectroscopy of later-type members.

Variable stars of α^2 CVn type are chemically peculiar with strong metal lines. This could imply a difference between the metallicity of the star and its atmosphere, an effect which we ignore. While HIP 115738’s variability is a generic problem for any isochrone analyses, the *Tycho* photometry is from a stack of 47 measurements (with a root-mean-square scatter in V_T of 0.029 mag). Stellar variability would be a much larger concern if we were to include non-simultaneous photometry at other wavelengths.

HIP 115738’s variability does, in principle, permit a measurement of the its rotational period. Unfortunately, there seems to be little agreement on the star’s photometric period among variability surveys, ranging from 2 hours (Rimoldini et al. 2012) to 1.4 days (Wraight et al. 2012). A rotation period of 2 hours is physically impossible for an A star of $\sim 2 R_{\odot}$.

An undisputed measurement of the stellar rotation period would enable us to constrain Ω , the stellar angular momentum. Unfortunately, the disagreement in measurements only allows us to place an upper limit of $\Omega/\Omega_{\text{crit}} \gtrsim 0.3$. HIP 115738 has a rotational $v \sin i = 30 \pm 8 \text{ km s}^{-1}$ (Abt & Morrell 1995). Constraining the star to be a very rapid rotator, $\Omega/\Omega_{\text{crit}} \gtrsim 0.6$, would therefore imply that it is seen nearly pole-on, and skew our age probability distributions towards youth.

The second panel of Figure 3 shows the results of our analysis for HIP 115738. These probability distributions are more difficult to interpret than for the other stars, given the uncertainty in the star’s rotation period and the possible metallicity bias on an α^2 CVn variable. If a slightly super-Solar metallicity is appropriate, and especially if HIP 115738 is a rapid rotator, the age probability distribution agrees well with the known age of AB Dor.

HIP 13209: The late B star HIP 13209 (41 Ari) is a consensus member of AB Dor (Zuckerman et al. 2011; Malo et al. 2013; Gagné et al. 2014). The star is a known spectroscopic binary and has been resolved at an angular separation of $\sim 0''.1$ (McAlister et al. 1987). The binary companion lacks a published spectral type or contrast, and was not seen in near-infrared adaptive optics imaging (Roberts et al. 2007; Janson et al. 2011). HIP 13209 has a measured rotational velocity of 175 km s^{-1} (Abt et al. 2002). The metallicity of AB Dor is somewhat uncertain, with measurements of $[\text{Fe}/\text{H}] = 0.02 \pm 0.02$ (Barenfeld et al. 2013) and $[\text{Fe}/\text{H}] = 0.10 \pm 0.03$ (Biazzo et al. 2012), from spectroscopy for later-type members.

HIP 13209 is the earliest-type member of AB Dor listed in Malo et al. (2013) and we include it here in spite of its companion. We address the unknown companion color and luminosity by presenting age probability distributions with three metallicity distributions, and also assuming no companion flux (solid histograms in Figure 3) and an F6V companion (dashed histograms in Figure 3). We use the F6 standard star π^3 Ori as our companion template in this case.

The third panel of Figure 3 shows the results for our three metallicity priors. With a Solar or slightly super-Solar metallicity, and with a mid F (or later) companion, our isochrone-based analysis agrees well with AB Dor’s known age.

HIP 116805: The late-B star κ And has been observed to host a substellar companion (Carson et al. 2013). The companion’s mass depends strongly on the host star’s age, which has been estimated from ~ 30 to ~ 300 Myr (Carson et al. 2013; Hinkley et al. 2013; Bonnefoy et al. 2014). The older age estimates are based on fitting nonrotating isochrones to the star’s position in color-luminosity space while the young age estimate relies on the star’s proposed membership in the Columba moving group (Malo et al. 2013). We revisit the stellar parameters using the formalism we develop in this paper.

We note that κ And does have a spectroscopic metallic-

ity measurement giving $[\text{Fe}/\text{H}] = -0.32 \pm 0.15$ (Wu et al. 2011). However, such a young, metal-poor star would be exceptional in the Solar neighborhood. Analyses of young clusters and moving groups, and of young stars in the local field, consistently find metallicities centered on or near the Solar value, with a dispersion ~ 0.1 dex (e.g. Gaidos & Gonzalez 2002; Biazzo et al. 2011, 2012). We therefore use the same three metallicity priors as for the other stars discussed above: $[\text{Fe}/\text{H}] = 0.1 \pm 0.05$, $[\text{Fe}/\text{H}] = 0.0 \pm 0.05$, and $[\text{Fe}/\text{H}] = -0.1 \pm 0.05$. The star has a rotational $v \sin i \approx 160 \text{ km s}^{-1}$ (Zorec & Royer 2012).

The bottom panel of Figure 3 shows our results for HIP 116805. A young age is excluded only if κ And’s metallicity is strongly sub-Solar. If its metallicity is approximately Solar or slightly super-Solar, HIP 116805’s position in color-magnitude space appears to be consistent with membership in Columba and a ~ 30 Myr age.

5.2. The Pleiades Open Cluster

The Pleiades open cluster is a large and extensively studied nearby stellar association. The Pleiades’ age is 130 ± 20 Myr, as measured from the lithium depletion boundary (Barrado y Navascués et al. 2004). It has also been estimated at 100 Myr using stellar isochrones without rotation (Meynet et al. 1993). Reddening for the bulk of the cluster is $E(B-V) = 0.04$ mags, with a slight variation from star to star (Vandenberg & Poll 1989; Taylor 2008). The distance to the Pleiades has been more controversial, but multiple lines of evidence, including several very precise parallax measurements, now point to ~ 135 pc (Pinsonneault et al. 1998; Pan et al. 2004; Soderblom et al. 2005; Melis et al. 2014). As a large, well-studied cluster, the Pleiades presents an important test of our statistical approach using the Georgy et al. (2013b) isochrones.

We restrict our analysis to late B Pleiads ($\sim 2.5 M_{\odot}$), HIP 17527, 17588, 17664, 17776, 17862, and 17900. These are similar in mass to the stars that we will later use in analyses of the Hyades open cluster and the Ursa Majoris moving group. They have evolved sufficiently in ~ 130 Myr to make an isochrone-based analysis possible, but are relatively far from the main-sequence turnoff. We adopt a parallax of 7.5 ± 0.2 mas (133 ± 4 pc) and a reddening of $E(B-V) = 0.04$ mag, with $R_V = 3.1$, for all stars. We use a metallicity of $[\text{Fe}/\text{H}] = 0.03 \pm 0.05$, as measured spectroscopically for 20 roughly Solar-type members (Soderblom et al. 2009).

Figure 4 shows our results. With a cluster $[\text{Fe}/\text{H}] = 0.03 \pm 0.05$, the marginalized probability distribution is $\sim 120 \pm 40$ Myr (1σ), completely consistent with age determinations using the lithium depletion boundary (Barrado y Navascués et al. 2004) or higher-mass turnoff stars (Meynet et al. 1993). Fixing the metallicity to $[\text{Fe}/\text{H}] = 0.03$ has little effect on the results, changing the 1σ uncertainty from ~ 40 to ~ 35 Myr.

The most massive Pleiads, HIP 17499 (Electra) and HIP 17702 (Alcyone), both strongly prefer an isochrone-based age of 110 ± 20 Myr (assuming the same distance and extinction). A few other stars (HIP 17608, 17489, and 17579) favor a slightly older age of ~ 300 Myr if we adopt $E(B-V) = 0.04$ mag. However, these stars appear to be somewhat more reddened than other Pleiads, with Breger (1984) giving $E(B-V)$ from 0.07 to 0.09 mag.

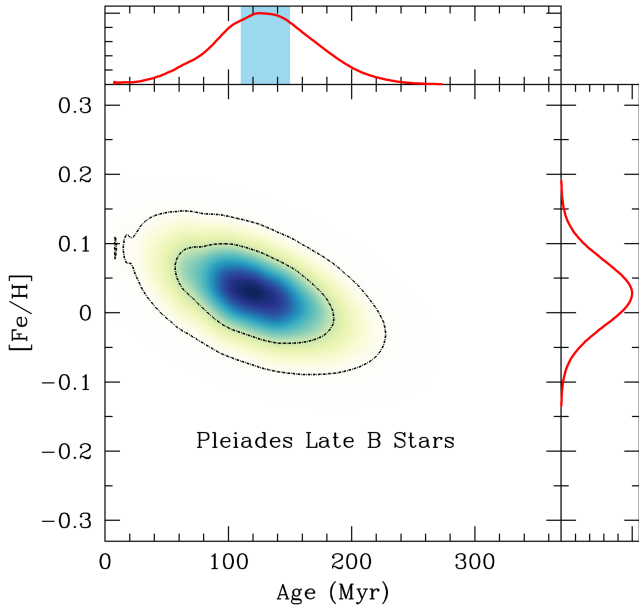


FIG. 4.— Posterior probability distribution in age and metallicity for the Pleiades, measured by fitting six late B stars, HIP 17527, 17588, 17664, 17776, 17862, and 17900, to the rotating stellar models of Georgy et al. (2013b). The cluster’s age has been measured to be 130 ± 20 Myr using the lithium depletion boundary (Barrado y Navascués et al. 2004); this interval is shaded light blue.

Adopting these values brings the ages for all Pleiades B-type stars into excellent agreement at ~ 110 – 120 Myr. The consistency of the rotating stellar models with the known age of the Pleiades lends credibility to our use of the same models, ~ 2 – $2.5 M_{\odot}$, to constrain the properties of the Ursa Majoris and Hyades clusters below.

5.3. The Ursa Majoris Moving Group

The Ursa Majoris moving group (UMa) is a coeval stellar association with an age of 500 ± 100 Myr derived from isochrone fits (King et al. 2003). As a coeval association, it is also expected to be chemically homogeneous. We can therefore apply the fitting techniques presented in this paper to early-type UMa stars, jointly constraining the association’s age and metallicity. For this exercise, we choose six early-type stars that are listed as UMa members in King et al. (2003): HIP 6061, 53910, 59774, 62956, 65477, and 76267. In the case of HIP 76267, we subtract the flux of its eclipsing binary companion (a G5V star, Tomkin & Popper 1986). HIP 65477 has an M-type companion (Mamajek et al. 2010) which is too faint to appreciably affect its optical and near-infrared flux (the largest effect, $\sim 1\%$ in K , is more than an order of magnitude smaller than the 2MASS uncertainty). We exclude the other early-type UMa members from King et al. (2003), all of which appear to be spectroscopic binaries with companions of unknown spectral type. Four of these six stars, HIP 53910, 59774, 62956, and 65477, are members of the UMa nucleus.

When fitting the ensemble of stars, we assume a Gaussian metallicity prior for the cluster centered on $[\text{Fe}/\text{H}] = 0$ with a dispersion of 0.1 dex. We assume the individual stars to have the (unknown) cluster value. Each individual star may have its own parallax, rotation and

orientation; we marginalize over all of these parameters star-by-star. We then multiply the joint posterior probability distributions in age and metallicity for all stars excluding HIP 6061, obtaining the results shown in Figure 5. The inner and outer contours enclose 68% and 95% of the probability, respectively. HIP 6061’s best-fit age is ~ 900 Myr by our analysis, and is highly inconsistent with an age of 600 Myr. The discrepancy may easily be removed if HIP 6061 is an unresolved binary, or a nonmember of the Ursa Majoris moving group (King et al. 2003 list it as a possible photometric member and a high-probability member largely based on its kinematics). All of the other stars are consistent with one another in their age-metallicity constraints, with their 1σ contours overlapping one another.

Our new isochrone analysis suggests that a slight revision to the age of UMa may be necessary, with a peak at ~ 600 Myr rather than ~ 500 Myr (King et al. 2003). The disagreement with the previously published age results mostly from the increase in main sequence lifetime with stellar rotation, which can be as large as ~ 25 – 30% (Ekström et al. 2012). Artificially removing this scaling (left contours, blue curves of 5) reduces the best-fit age for UMa to ~ 500 Myr, in excellent agreement with the earlier, nonrotating isochrone fits. Our isochrone analysis also favors a very slightly super-Solar metallicity, in agreement with recent spectroscopic measurements of later-type members. Tabernero et al. (2014), using a sample of 44 candidate FGK members, find that 29 of the 44 stars share a similar chemical composition, with $[\text{Fe}/\text{H}] = 0.03 \pm 0.07$ dex.

5.4. The Hyades Open Cluster

We now revisit the age of the Hyades open cluster, calculated to be 625 ± 50 Myr by Perryman et al. (1998) using nonrotating isochrones with convective overshooting. The Perryman et al. (1998) constraint is based mostly on five stars near the main-sequence turnoff without indications of multiplicity: HIP 20542, 20635, 21029, 21683, and 23497. Reddening between the Sun and the Hyades is negligible (Taylor 2006). We use the same five stars in our present framework to place new constraints on the Hyades age, adopting a metallicity of $[\text{Fe}/\text{H}] = 0.10$ (Taylor & Joner 2005) with a conservative Gaussian error of 0.05 dex. We also add the individual components of the binary HIP 20894 as two additional stars, with a magnitude difference $\Delta V_T = 1.10$ and $\Delta(B_T - V_T) = -0.006$ (Peterson et al. 1993). As for Ursa Majoris, we assume the stars to share a composition and marginalize over mass, rotation, and orientation separately for each star.

The lengthening of the main-sequence lifetime with rotation maps onto a much older inferred age of ~ 950 Myr for the Hyades, shown in Figure 6. As Figure 2 shows, a rotating isochrone can also overlap a slightly more massive nonrotating isochrone near the main sequence turnoff. Indeed, the difference between the maximum likelihood masses with and without including rotation is typically ~ 0.05 – $0.1 M_{\odot}$, which corresponds to a $\sim 10\%$ difference in main-sequence lifespan. The left and right density plots in Figure 6 show the effect of the increase in time spent on the main sequence, which increases the best-fit age from ~ 750 Myr to ~ 950 Myr. Removing the difference in mass, and the resulting difference in main sequence lifespan, would bring the left density plot (with-

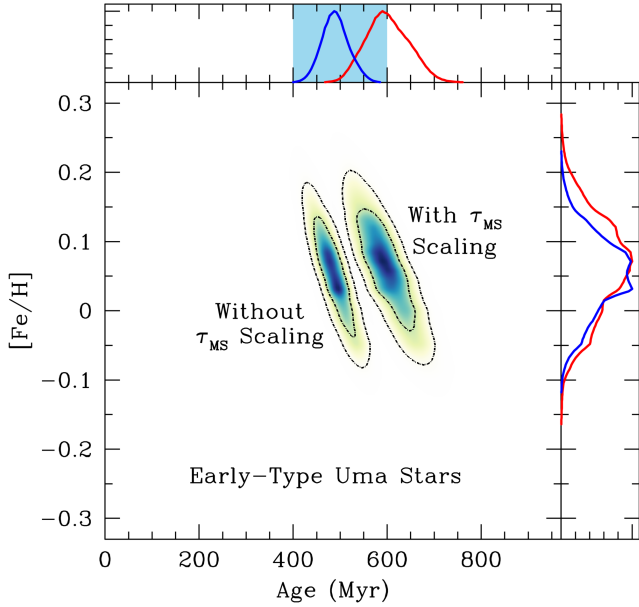


FIG. 5.— Joint posterior probability distribution for the age and metallicity of five early-type Ursa Majoris moving group members, with a metallicity prior of $[\text{Fe}/\text{H}] = 0 \pm 0.1$. We have excluded HIP 6061 from these curves; its age distribution, centered on ~ 900 Myr, is incompatible with the other five stars, HIP 53910, 59774, 62956, 65477, and 76267. When artificially removing the increase in main-sequence lifetime with rotation (left contours, blue curves), our derived age of 500 ± 100 Myr matches the value derived in King et al. (2003). We shade the previously determined age light blue for comparison. The best-fit age with our current treatment is slightly older, ~ 600 Myr. The best-fit age changes little if we apply a slightly stronger metallicity constraint of $[\text{Fe}/\text{H}] = 0.03 \pm 0.07$ measured in FGK candidate UMa members (Tabernero et al. 2014).

out the age scaling) into good agreement with previously derived ages.

All seven turnoff stars, including the two components of HIP 20894, are consistent with an age of ~ 950 Myr. The 800 Myr Z_{\odot} isochrone in Ekström et al. (2012) has its red clump at $B - V \approx 1$, and $V \approx 0.4$, completely consistent with the location of the four red giants in Figure 21 of Perryman et al. (1998). In the nonrotating PARSEC isochrones, increasing the metallicity from Z_{\odot} to $[\text{Fe}/\text{H}] = 0.1$ extends the main-sequence lifetimes by $\sim 5\%$, hinting that the red clump at $[\text{Fe}/\text{H}] = 0.1$ and $\tau \approx 950$ Myr may also fit the observed Hyades red giants.

Open clusters like the Hyades are often used as benchmarks to calibrate age dating techniques for lower mass stars. If the cluster’s age really is closer to 900 Myr than to 600 Myr, it may require a re-calibration of secondary age indicators like stellar rotation and activity (Mamajek & Hillenbrand 2008). Alternatively, if the younger age is correct, it indicates serious problems with the new, rotating isochrones. This could entail a large overestimate of the amount of additional hydrogen supplied to the core by rotational mixing, or compensating changes in other processes like overshooting. At the very least, our results suggest that the uncertainty in the Hyades’ age is significantly underestimated. Resolving the discrepancy might require other age indicators for these stars or additional tests of the rotating stellar models. Asteroseismology of lower-mass stars provides a relatively

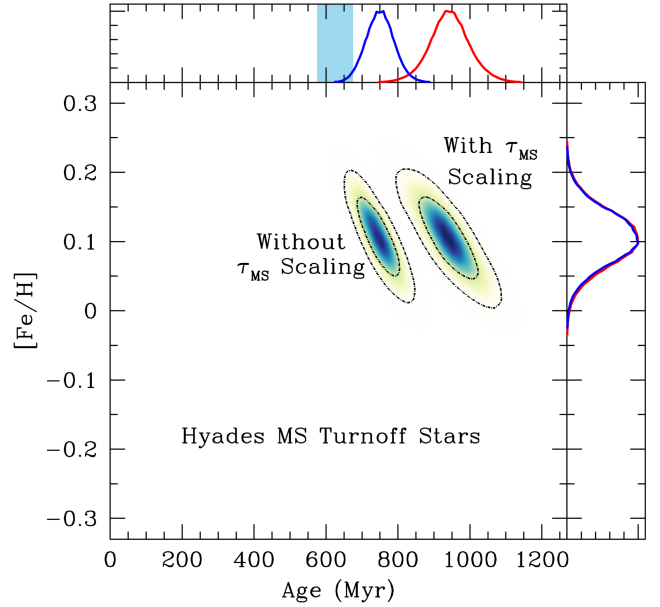


FIG. 6.— Age-metallicity constraints on the Hyades open cluster using seven main-sequence turnoff members (HIP 20542, 20635, 21029, 21683, 23497 and the two components of HIP 20894). The inner and outer contours enclose 68% and 95% of the probability, respectively; the left contours have had the increase in main-sequence lifespan with stellar rotation artificially removed. The best-fit age at $[\text{Fe}/\text{H}] = 0.1$ is ~ 950 Myr, much older than the consensus age of 625 Myr, which was calculated largely based on five of these seven stars (Perryman et al. 1998). We shade the previous age constraint in light blue for comparison. Most of this increase comes from the lengthening of the main sequence timescale with rotation, the difference between the red and blue curves. A rapidly rotating turnoff star also overlaps a more massive (and shorter-lived) nonrotating star in the color-magnitude diagram (Figure 2). This effect further increases the estimated age, accounting for the fact that the blue curve is still $\sim 15\%$ older than the consensus age of the Hyades. Either the Hyades are much older than currently thought, or the modeling of stellar rotation must be revisited.

direct measurement of the central sound speed, and by extension, the mean molecular weight and helium fraction. The Transiting Exoplanet Survey Satellite (TESS, Ricker et al. 2014) could soon provide crucial data for F and G-type Hyades members.

6. CONCLUSIONS

In this paper, we have used recently computed stellar models with an improved treatment of stellar rotation (Georgy et al. 2013b) to derive stellar parameters, particularly ages, of nearby early-type stars. We combine ATLAS9 model atmospheres (Castelli & Kurucz 2004) with the two-dimensional model of T_{eff} and $\log g$ in LR11 to compute synthetic magnitudes as a function of orientation. We then use fine grids of nonrotating isochrones (Girardi et al. 2002) to interpolate between the rotating models in time, mass, and metallicity. In the case of metallicity, we also use the nonrotating models to *extrapolate* the rotating models to super-Solar metallicities.

We have applied a Bayesian age analysis to obtain posterior probability distributions of the stellar parameters assuming random orientations and a standard initial mass function. While we have computed synthetic photometry through a wide range of filters, the analysis we present relies only on the *Tycho* $B_T V_T$ system

and *Hipparcos* parallaxes (ESA 1997). The photometry and astrometry, which have since been updated (Høg et al. 2000; van Leeuwen 2007), provide uniform and high-quality data for all bright stars.

We have applied our analysis first to stars with known ages, including the Pleiades open cluster. Our use of the new rotating isochrones recovers, within its errors, the known ages of β Pictoris and (with caveats) two members of the AB Doradus moving group. Fitting of the late B Pleiads and the most massive cluster members each recovers an age of ~ 110 – 120 Myr for the association (with a 1σ error of ~ 40 Myr when using only late B members). This is in good agreement with previous results using both isochrone fitting and the lithium depletion boundary (Meynet et al. 1993; Barrado y Navascués et al. 2004).

Fitting ~ 2 – $2.5 M_{\odot}$ models to the Ursa Majoris moving group and the Hyades open cluster implies older ages than previously derived. For UMa, we derive an age of 600 ± 100 Myr, in slight tension with the previous isochrone-based age of 500 ± 100 Myr (King et al. 2003). The difference is much starker for the Hyades, previously dated to 625 ± 50 Myr using main-sequence turnoff stars (Perryman et al. 1998). Using the same turnoff stars, we find that all are consistent with a much older age of 950 ± 100 Myr, and are inconsistent with ~ 650 Myr. This results from an increase in both main-sequence lifetime and luminosity due to rotational mixing.

The older age we derive for the Hyades turnoff stars raises questions about either the cluster’s age, stellar

modeling, or both. Including stellar modeling uncertainties could imply a much larger error for the cluster age, perhaps 800 ± 200 Myr, which would propagate into secondary age indicators calibrated on clusters like the Hyades. Resolving these modeling uncertainties will likely require independent age indicators, perhaps asteroseismology of F and G type Hyades stars.

Finally, we provide a web interface at www.bayesianstellarparameters.info where a user may obtain the posterior probability distributions of age, mass, and orientation for any bright ($H_P < 9$), blue ($B - V < 0.25$) *Hipparcos* star with a good distance ($\varpi/\sigma_{\varpi} > 10$). The web server currently assumes negligible extinction and uses only *Tycho* $B_T V_T$ photometry and *Hipparcos* parallaxes. A careful analysis would be needed to place other photometry, like 2MASS, on the same absolute scale, and ensure that the resulting ages remain consistent with one another and with independently determined ages.

The authors would like to thank the computing staff at the Institute for Advanced Study for help in setting up a web interface, Waqas Bhattachi for the server script template, and Josh Schlieder for helpful comments on the manuscript. This work was performed in part under contract with the Jet Propulsion Laboratory (JPL) funded by NASA through the Sagan Fellowship Program executed by the NASA Exoplanet Science Institute.

REFERENCES

- Abt, H. A., Levato, H., & Grosso, M. 2002, *ApJ*, 573, 359
 Abt, H. A., & Morrell, N. I. 1995, *ApJS*, 99, 135
 Anders, E., & Grevesse, N. 1989, *Geochim. Cosmochim. Acta*, 53, 197
 Asplund, M., Grevesse, N., Sauval, A. J., & Scott, P. 2009, *ARA&A*, 47, 481
 Aufdenberg, J. P., Mérand, A., Coudé du Foresto, V., et al. 2006, *ApJ*, 645, 664
 Barenfeld, S. A., Bubar, E. J., Mamajek, E. E., & Young, P. A. 2013, *ApJ*, 766, 6
 Barnes, S. A. 2003, *ApJ*, 586, 464
 Barnes, S. A. 2007, *ApJ*, 669, 1167
 Barrado y Navascués, D., Stauffer, J. R., & Jayawardhana, R. 2004, *ApJ*, 614, 386
 Barrado y Navascués, D., Stauffer, J. R., Song, I., & Caillault, J.-P. 1999, *ApJ*, 520, L123
 Bessell, M., & Murphy, S. 2012, *PASP*, 124, 140
 Biazzo, K., D’Orazi, V., Desidera, S., et al. 2012, *MNRAS*, 427, 2905
 Biazzo, K., Randich, S., Palla, F., & Briceño, C. 2011, *A&A*, 530, A19
 Binks, A. S., & Jeffries, R. D. 2014, *MNRAS*, 438, L11
 Bonnefoy, M., Currie, T., Marleau, G.-D., et al. 2014, *A&A*, 562, A111
 Breger, M. 1984, *A&A*, 137, 145
 Carson, J., Thalmann, C., Janson, M., et al. 2013, *ApJ*, 763, L32
 Casagrande, L., Schönrich, R., Asplund, M., et al. 2011, *A&A*, 530, A138
 Castelli, F., & Kurucz, R. L. 2004, *ArXiv Astrophysics e-prints*, astro-ph/0405087
 Chabrier, G. 2003, *PASP*, 115, 763
 Chiappini, C., Romano, D., & Matteucci, F. 2003, *MNRAS*, 339, 63
 Claret, A. 1998, *A&AS*, 131, 395
 Connelly, J. N., Bizzarro, M., Krot, A. N., et al. 2012, *Science*, 338, 651
 Cutri, R. M., Skrutskie, M. F., van Dyk, S., et al. 2003, 2MASS All Sky Catalog of point sources.
 Dotter, A., Chaboyer, B., Jevremović, D., et al. 2008, *ApJS*, 178, 89
 Ekström, S., Georgy, C., Eggenberger, P., et al. 2012, *A&A*, 537, A146
 ESA, ed. 1997, *ESA Special Publication*, Vol. 1200, The HIPPARCOS and TYCHO catalogues. Astrometric and photometric star catalogues derived from the ESA HIPPARCOS Space Astrometry Mission
 Espinosa Lara, F., & Rieutord, M. 2011, *A&A*, 533, A43
 Gagné, J., Lafrenière, D., Doyon, R., Malo, L., & Artigau, É. 2014, *ApJ*, 783, 121
 Gaidos, E. J., & Gonzalez, G. 2002, *New Astron.*, 7, 211
 Georgy, C., Ekström, S., Eggenberger, P., et al. 2013a, *A&A*, 558, A103
 Georgy, C., Ekström, S., Granada, A., et al. 2013b, *A&A*, 553, A24
 Georgy, C., Granada, A., Ekström, S., et al. 2014, *A&A*, 566, A21
 Girardi, L., Bertelli, G., Bressan, A., et al. 2002, *A&A*, 391, 195
 Glatzmaier, G. A. 1985, *ApJ*, 291, 300
 Hempelmann, A., Schmitt, J. H. M. M., Schultz, M., Ruediger, G., & Stepien, K. 1995, *A&A*, 294, 515
 Hinkley, S., Pueyo, L., Faherty, J. K., et al. 2013, *ApJ*, 779, 153
 Høg, E., Fabricius, C., Makarov, V. V., et al. 2000, *A&A*, 355, L27
 Janson, M., Bonavita, M., Klahr, H., et al. 2011, *ApJ*, 736, 89
 King, J. R., Villarreal, A. R., Soderblom, D. R., Gulliver, A. F., & Adelman, S. J. 2003, *AJ*, 125, 1980
 Kroupa, P. 2001, *MNRAS*, 322, 231
 Lagrange, A.-M., Gratadour, D., Chauvin, G., et al. 2009, *A&A*, 493, L21
 Lebreton, Y., Goupil, M.-J., & Montalbán, J. 2014, *ArXiv e-prints*, 1410.5336
 Li, C., de Grijs, R., & Deng, L. 2014, *Nature*, 516, 367
 Luhman, K. L., Stauffer, J. R., & Mamajek, E. E. 2005, *ApJ*, 628, L69
 Malo, L., Doyon, R., Feiden, G. A., et al. 2014, *ApJ*, 792, 37
 Malo, L., Doyon, R., Lafrenière, D., et al. 2013, *ApJ*, 762, 88
 Mamajek, E. E., & Bell, C. P. M. 2014, *ArXiv e-prints*, 1409.2737
 Mamajek, E. E., & Hillenbrand, L. A. 2008, *ApJ*, 687, 1264
 Mamajek, E. E., Kenworthy, M. A., Hinz, P. M., & Meyer, M. R. 2010, *AJ*, 139, 919
 McAlister, H. A., Hartkopf, W. I., Hutter, D. J., & Franz, O. G. 1987, *AJ*, 93, 688
 Melis, C., Reid, M. J., Mioduszewski, A. J., Stauffer, J. R., & Bower, G. C. 2014, *Science*, 345, 1029
 Meynet, G., & Maeder, A. 2000, *A&A*, 361, 101
 Meynet, G., Mermilliod, J.-C., & Maeder, A. 1993, *A&AS*, 98, 477
 Nielsen, E. L., Liu, M. C., Wahhaj, Z., et al. 2013, *ApJ*, 776, 4

- Nieva, M.-F., & Przybilla, N. 2012, *A&A*, 539, A143
- Noyes, R. W., Hartmann, L. W., Baliunas, S. L., Duncan, D. K., & Vaughan, A. H. 1984, *ApJ*, 279, 763
- Ortega, V. G., Jilinski, E., de La Reza, R., & Bazzanella, B. 2007, *MNRAS*, 377, 441
- Pan, X., Shao, M., & Kulkarni, S. R. 2004, *Nature*, 427, 326
- Parker, E. N. 1955, *ApJ*, 122, 293
- Perryman, M. A. C., Brown, A. G. A., Lebreton, Y., et al. 1998, *A&A*, 331, 81
- Peterson, D. M., Stefanik, R. P., & Latham, D. W. 1993, *AJ*, 105, 2260
- Pietrinferni, A., Cassisi, S., Salaris, M., & Castelli, F. 2004, *ApJ*, 612, 168
- Pinsonneault, M. H., Stauffer, J., Soderblom, D. R., King, J. R., & Hanson, R. B. 1998, *ApJ*, 504, 170
- Preston, G. W. 1974, *ARA&A*, 12, 257
- Przybilla, N., Nieva, M.-F., & Butler, K. 2008, *ApJ*, 688, L103
- Ricker, G. R., Winn, J. N., Vanderspek, R., et al. 2014, in *Society of Photo-Optical Instrumentation Engineers (SPIE) Conference Series*, Vol. 9143, *Society of Photo-Optical Instrumentation Engineers (SPIE) Conference Series*, 20
- Rimoldini, L., Dubath, P., Süveges, M., et al. 2012, *MNRAS*, 427, 2917
- Roberts, L. C., Jr., Turner, N. H., & ten Brummelaar, T. A. 2007, *AJ*, 133, 545
- Roy, J.-R., & Kunth, D. 1995, *A&A*, 294, 432
- Royer, F., Zorec, J., & Gómez, A. E. 2007, *A&A*, 463, 671
- Salpeter, E. E. 1955, *ApJ*, 121, 161
- Schröder, C., Reiners, A., & Schmitt, J. H. M. M. 2009, *A&A*, 493, 1099
- Sestito, P., & Randich, S. 2005, *A&A*, 442, 615
- Smith, K. C. 1996, *Ap&SS*, 237, 77
- Soderblom, D. R. 2010, *ARA&A*, 48, 581
- Soderblom, D. R., Laskar, T., Valenti, J. A., Stauffer, J. R., & Rebull, L. M. 2009, *AJ*, 138, 1292
- Soderblom, D. R., Nelan, E., Benedict, G. F., et al. 2005, *AJ*, 129, 1616
- Tabernero, H. M., Montes, D., Gonzalez Hernandez, J. I., & Ammler-von Eiff, M. 2014, *ArXiv e-prints*, 1409.2348
- Takeda, G., Ford, E. B., Sills, A., et al. 2007, *ApJS*, 168, 297
- Taylor, B. J. 2006, *AJ*, 132, 2453
- Taylor, B. J. 2008, *AJ*, 136, 1388
- Taylor, B. J., & Jone, M. D. 2005, *ApJS*, 159, 100
- Tomkin, J., & Popper, D. M. 1986, *AJ*, 91, 1428
- Valenti, J. A., & Fischer, D. A. 2005, *ApJS*, 159, 141
- van Belle, G. T., Ciardi, D. R., ten Brummelaar, T., et al. 2006, *ApJ*, 637, 494
- van Leeuwen, F. 2007, *A&A*, 474, 653
- Vandenberg, D. A., & Poll, H. E. 1989, *AJ*, 98, 1451
- von Zeipel, H. 1924, *MNRAS*, 84, 684
- Wilson, O. C. 1963, *ApJ*, 138, 832
- Wraight, K. T., Fossati, L., Netopil, M., et al. 2012, *MNRAS*, 420, 757
- Wu, Y., Singh, H. P., Prugniel, P., Gupta, R., & Koleva, M. 2011, *A&A*, 525, A71
- Yi, S., Demarque, P., Kim, Y.-C., et al. 2001, *ApJS*, 136, 417
- Zahn, J.-P. 1992, *A&A*, 265, 115
- Zorec, J., & Royer, F. 2012, *A&A*, 537, A120
- Zuckerman, B., Rhee, J. H., Song, I., & Bessell, M. S. 2011, *ApJ*, 732, 61
- Zuckerman, B., Song, I., Bessell, M. S., & Webb, R. A. 2001, *ApJ*, 562, L87